Hierarchical tannin-derived carbons as efficient tetracycline adsorbents

Rafael Luan Sehn Canevesi, Angela Sanchez-Sanchez, Philippe Gadonneix, Alain Celzard, V. Fierro

Hierarchical tannin-derived carbons as efficient tetracycline adsorbents

R.L.S. Canevesi, A. Sanchez-Sanchez, P. Gadonneix, A. Celzard, V. Fierro*

IJL UMR 7198 CNRS, Université de Lorraine, 88000 Epinal, France

* Corresponding author: vanessa.fierro@univ-lorraine.fr

Abstract

Mimosa tannin has been used to produce two different types of carbons materials: hydrothermal carbon (HTC) on the one hand, and ordered mesoporous carbon (OMC) on the other hand. Both were obtained after pyrolysis at 1173 K, resulting in materials with similar BET areas, close to 580 m^2/g, but very different pore size distributions (PSDs). HTC was essentially microporous while OMC had a large fraction of mesopores. Tetracycline (TC) adsorption on these carbons was studied at equilibrium but kinetics experiments were also carried out at two different temperatures. The TC adsorption data were fitted by different mathematical, classical models, and new kinetic models were introduced to take into account their very different PSDs. While the two materials presented similar BET areas (A_{BET}), the OMC had a TC adsorption capacity six times higher than that of the HTC. Adsorption kinetics were also strongly affected by the PSD. The importance of having high accessible pore volumes and not only high surface areas in order to have good performances in TC adsorption has been evidenced not only with our materials but also in the light of the TC adsorption data reported in the open literature. We proved that A_{BET}, while easy to calculate and always reported, is not the best tool to assess the potential suitability of an adsorbent to the removal of aqueous pollutants.

Key words: Kinetics modelling; Soft-templating; Tetracycline adsorption; Mesoporous carbons; Tannin

1. INTRODUCTION

Antibiotics like tetracycline (TC) are frequently used to treat bacterial infections, as food additives, and to keep the control of microbiological growth in industry [1]. In fact, TC is one of the most used antibiotics, due its low price and broad spectrum of antimicrobial activity [2]. However, its massive use and inefficient management have led to substantial accumulations in the environment [3]. The main problem lies in the ineffective absorption of TC by the body, which means that 30 to 90% of the ingested TC is evacuated and ends up in wastewater, which traditional treatments fail to eliminate [2,4,5]. As a consequence, antibiotics such as TC are found in water bodies, which is dangerous because they are designed to have a biological effect but also because their presence could increase the number of bacteria resistant to antibiotics [6,7].

Several methods are applied to treat wastewater and remove antibiotics residues, such as ozonation [8,9], electrocoagulation [10,11], biodegradation [12,13], membrane separation [14,15], advanced oxidation process [16,17] and adsorption [18–20]. Adsorption is a very competitive process that allows pharmaceutical compounds removal from aqueous solutions due to its ease of use and low cost compared to other methods [21]. Nevertheless, in the adsorption process, the critical parameter that makes it work well or not is the selection of the adsorbent [22]. In this way, several adsorbents have been applied for the removal of pharmaceutical compounds, such as zeolites [23], metal organic frameworks (MOFs) [24] and activated carbons [25]. The latter are porous materials with highly developed pore texture, large surface areas and a broad variety of functional groups [26,27]. Biomass such as algae [28], rice crops byproducts [29–32], lignin [33], and others [25,34–37] have been used as adsorbents to prevent water contamination from various types of pharmaceutical and personal care products (PPCPs). Activated carbons can be produced by “physical” or “chemical” routes, both methods increasing the surface area but requiring either a second step of

activation after pyrolysis (for physical activation) or extensive washing (for chemical activation).

Different methodologies, such as hydrothermal carbonisation or templating have been implemented to increase the heteroatoms content or the mesopore volume, respectively. Hydrothermal carbonisation implies the treatment of precursors in aqueous solution at moderates temperatures and under self-generated pressures [38,39]. Soft-templating [40] and hard-templating [41,42] allow the production of micro-mesoporous carbons after pyrolysis of a mesophase or a composite, respectively. In the case of hard-templating, the resultant carbon is a negative replica of the template. In the case of soft-templating, an amphiphilic surfactant, usually a triblock copolymer, is used in solution to form micelles that act as porogen in the carbon precursor. A subsequent pyrolysis then eliminates the surfactant, producing mesoporosity in the final carbon material. Soft-templating became popular because it is a less expensive, simpler and greener method than hard-templating [43], for which silica or zeolite is used as a template and must be removed after pyrolysis, using hazardous chemicals such as HF [44].

Due to the low cost and high availability of carbon precursors, the application of porous carbon materials to clean water streams containing TC has increased. The affinity of carbon materials produced from several precursors and different methodologies have been tested. Some biochars produced from ground coffee [45], loblolly pine [46] and others [47,48] have shown TC adsorption capacities up to 593 mg g^{-1}. Hydrothermal carbons produced by different precursors (e.g. American agave [25], orange peels [49] and others biomass [50,51]), and templated carbon materials produced from various templates (e.g. silicas [52,53], zeolites [54] and MOFs [55]) have been used to eliminate PPCPs. Some of these carbon materials [25] exhibited tetracycline adsorption capacities above 50 mg g^{-1}.

92 Tannins are traditionally used in several industrial domains (e.g. leather [56], food [57,58],
93 medicine [59,60] and others [61,62]). However, in recent years, their use has been extended to
94 the manufacture of environment-friendly products (e.g. resins [63–65], foams [66–69] and
95 others [70–72]). They have also been applied to the production of ordered mesoporous
96 carbons (OMCs) and hydrothermal carbons (HTCs) [73], because the tannins in question here
97 are essentially based on flavonoid-type polyphenols, which have a good carbon yield after
98 crosslinking [74] and are easy to enrich with nitrogen [75]. Mimosa tannins (MT) in particular
99 have been used as precursors of OMCs and HTCs for several applications (e.g.
100 supercapacitors [74,76–78] and adsorbents [25]).

101 Mathematical modelling is a relevant tool to evaluate the adsorption efficiency and to
102 determine which phenomena play a role in the adsorption process [79]. Thus, depending on
103 the adsorbent characteristics (e.g. presence or absence of a hierarchical structure) or the
104 process conditions (e.g. temperature and stirring speed), the kinetics of the process can be
105 controlled by one or more phenomena simultaneously [80]. In the literature, there are different
106 models that consider a single phenomenon acting during adsorption (e.g. pseudo first [81] or
107 second order [82]), or two phenomena occurring in series (e.g dual resistance models [19]).
108 However, there is a lack of models that consider the existence of different phenomena acting
109 simultaneously in a parallel way.

110 The present study aimed at comparing two different carbon materials produced from
111 mimosa tannins (MT), obtained by a first step of either hydrothermal treatment or soft-
112 templating, and followed by pyrolysis. No additional activation step has been applied. The
113 resultant textural and chemical proprieties of both kinds of adsorbents were very different,
114 and they have been studied to understand their performance in the adsorption of TC.
115 Depending of the material, the kinetics of TC adsorption were adequately predicted taking

into account the diffusion resistance in micropores or a combined diffusion resistance in micropores and mesopores.

2. MATERIAL AND METHODS

2.1. Materials preparation

Two kinds of carbon materials were prepared using mimosa tannin (MT) as carbon precursor by applying hydrothermal carbonisation or soft-templating followed by pyrolysis. The production methodologies of hydrothermal carbons (HTCs) were explained in detail by Braghiroli et al [75] (see Fig. 1). In short, 4g of MT were dissolved in 40 mL of water. The solution was poured in a Teflon-lined autoclave, which was hermetically closed and placed in an oven at 453 K for 24 h. The recovered hydrochar was submitted to pyrolysis at 1173 K under nitrogen atmosphere, using a constant heating rate of 1 K min^{-1} up to the final temperature, which was held for 1 hour. Finally, the sample was cooled under nitrogen atmosphere.

Soft templating was performed using the surfactant Pluronic PE 6800® as pore-directing agent. The method is similar to that reported by Sanchez-Sanchez et al [78] (see Fig. 1). In short, 4g of MT were dissolved in 16 mL of water and 4g of Pluronic PE 6800® were dissolved in other 16 mL of water. The two solutions were then poured together in a glass vial and placed in a thermostatic bath at 303 K for 3 h. After this time, phase separation occurred. The supernatant was separated and eliminated, and the solid fraction was dried in an oven at 333 K for 12 h, before subjecting it to pyrolysis. The mesophase was heated at 1 K min^{-1} until 673 K, a temperature maintained for 4 h, followed by a second ramp of 2 K min^{-1} until 1173 K, maintained for 1 h. Heating, pyrolysis and cooling were carried out under nitrogen atmosphere.

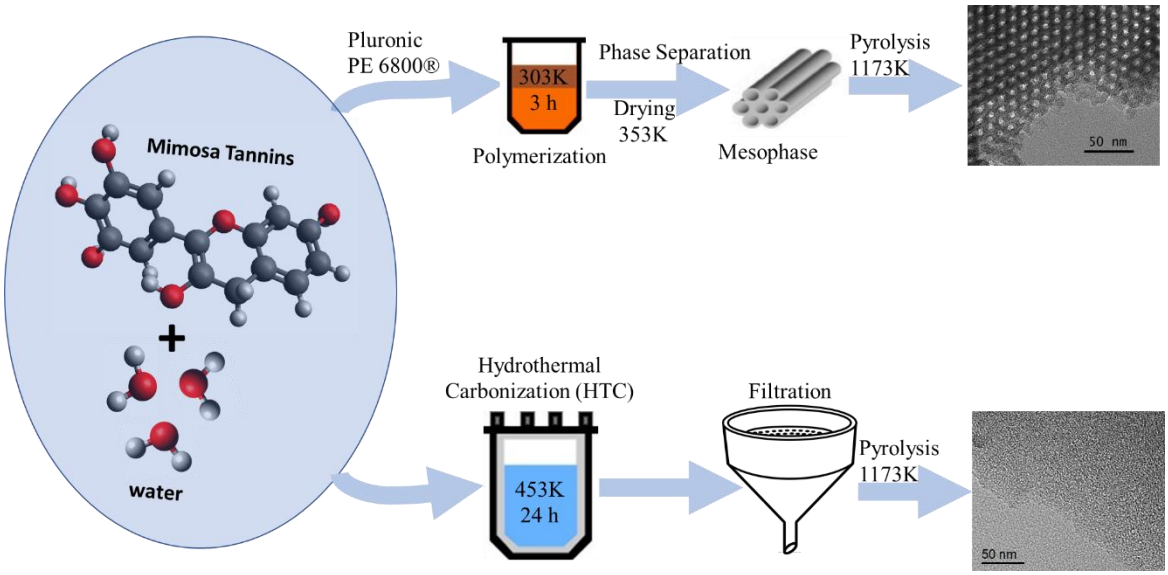

Figure 1. Scheme of the synthesis of the tannin-based carbon materials.

2.2. Materials characterisation

The elemental composition of the HTC and OMC materials in terms of hydrogen, carbon, oxygen, nitrogen and sulphur contents (wt. %) was determined using a CHONS elemental analyser (Vario EL Cube, Elementar). Infrared spectra were obtained in the range of wavenumbers 600-4000 cm^{-1} using a Fourier-Transform Infrared (FTIR) spectrometer (Frontier Spotlight 400, Perkin-Elmer).

Small-angle X-ray diffraction (XRD) patterns were recorded with a Panalytical X'Pert Pro diffractometer. The latter was equipped with a Cu (K_α radiation) anticathode and a high-speed multichannel X'Celerator detector (scanning range 2θ = 0.4 – 4°; step size = 0.01671°; time per step size = 1.26 s), and was used in Bragg–Brentano configuration in reflection mode. The interplanar distance, d_{100} (nm), was calculated by applying Eq. (1):

$$n \cdot \lambda = 2d_{100}sin(\theta) \quad (1)$$

where n is a positive integer (we assume n = 1), λ is the wavelength (0.15418 nm) of the incident radiation, and θ is the Bragg angle.

The unit cell parameter (a, nm) of the carbon mesostructure was calculated by applying Eq. (2):

$$a = \frac{2}{\sqrt{3}} d_{100} \quad (2)$$

where d_{100} (nm) is the interplanar spacing obtained from XRD patterns.

The pH at which the net surface charge is zero, called point of zero charge (pH_{PZC}), is affected by the nature and amount of functional groups existing on the surface of the materials. Six 0.1 mol L^{-1} aqueous solutions of $NaNO_3$ were prepared and the pH was adjusted using either NaOH or HCl to values ranging from 2 and 12 by steps of two pH units. In each solution, 25 mg of carbon were added and left under stirring for 24 h to obtain the pH at equilibrium. The latter was measured and the difference between its value and the initial one was plotted against the initial pH. The pH at which the curve goes through zero was taken as the pH_{PZC} [83].

The textural properties of the two carbons were determined by adsorption of nitrogen and carbon dioxide at 77 K and 273 K, respectively, using ASAP 2020 and ASAP 2040 automatic adsorption devices (Micromeritics), respectively. The BET area, A_{BET} (m^2 g^{-1}), was calculated by applying the BET (Brunauer-Emmet-Teller) method [84]. All the calculations were done with the MicroActive® software provided by Micromeritics. The pore size distribution (PSD) was determined by applying the non-local density functional theory (NLDFT), combining both N_2 and CO_2 adsorption isotherms by the SAIEUS® software provided by Micromeritics. We applied the 2D version of this theory, which takes into account heterogeneous surface (2D_NLDFT-HS) [85,86]. The PSD results were used to calculate the following parameters: the specific surface area, S_{NLDFT} (m^2 g^{-1}); the total pore volume V_T (cm^3 g^{-1}); volume and surface area of ultramicropores (pore size below 0.7 nm), $V_{u\mu}$ (cm^3 g^{-1}) and $S_{u\mu}$ (m^2 g^{-1}), respectively; volume and surface area of supermicropores (pore size between 0.7 and 2 nm)

$V_{s\mu}$ ($cm^3\ g^{-1}$) and $S_{s\mu}$ ($m^2\ g^{-1}$), respectively; volume and surface area of micropores (by summing the super- and ultra-micropore volumes and areas), V_μ ($cm^3\ g^{-1}$) and S_μ ($m^2\ g^{-1}$), respectively; and surface area of mesopores (by subtracting the micropore area from S_{NLDFT}), S_m ($m^2\ g^{-1}$).

The kinetics and equilibrium studies of tetracycline adsorption (CAS 60-54-8, 98% pure, provided by Sigma Aldrich) were carried out in a batch system. The adsorption isotherms, at 288 and 308 K, were done as follow: 25 mL of tetracycline (TC) solutions at concentrations ranging from 10 to 500 mg L^{-1}, at pH 6, were brought into contact with 25 mg of carbon in a tightly closed flask under stirring for 24 h.

The adsorption kinetics were determined at 288 and 308 K using 25 mg of carbon and 25 mL of TC solution at a concentration of 500 mg L^{-1}, at pH 6. Eight data points of concentration as a function of contact time were recorded, the contact time varying between 15 min and 24 h.

The TC concentrations of the solutions were measured, after filtration with a Nylon® membrane with a pore diameter of 0.25 µm, by UV-vis spectrometry at a wavelength of 358 nm (Lambda 35 Perkin Elmer).

2.3. Mathematical modelling of TC adsorption

2.3.1. Adsorption kinetics

The pseudo-first order (PFO) kinetics model was first proposed by Lagergren [81] and is generally applied to liquid-phase adsorption [87]. The PFO model is represented by the following equation:

$$\frac{dq_t}{dt} = k_1\left(q_{eq} - q_t\right) \quad (3)$$

where q_t and q_{eq} (mg g^{-1}) are the amounts adsorbed at time t and at equilibrium, respectively, and k_1 (h^{-1}) is the PFO constant.

The pseudo-second order (PSO) kinetics model is also largely used to describe adsorption in the liquid phase [87]. This model was first proposed by Ho and McKay [82]. The PSO model is described by the following equation:

$$\frac{dq_t}{dt} = k_2\left(q_{eq} - q_t\right)^2 \quad (4)$$

where k_2 (g mg^{-1} h^{-1}) is the PSO rate constant.

The dual resistance model (DRM) considers that resistance to external mass transfer and intraparticle diffusion simultaneously affect the adsorption kinetics. The resistance to external mass transfer is generally associated with the existence of a layer of fluid around the adsorbent, which could be represented as a liquid film where the solute diffuses from the solution (C_t, mg L^{-1}) to the adsorbent surface (where the local concentration is C_s, mg L^{-1}). Mathematically, this can be represented by a linear expression where the driving force is the solute concentration gradient ($C_t - C_s$), according to:

$$\frac{dq_t}{dt} = k_F(C_t - C_s) \quad (5)$$

where k_F (L g^{-1} h^{-1}) is the coefficient of mass transfer in the liquid film between the boundary layer and the adsorbent surface.

The intraparticle diffusion of TC in the carbon micropores was evaluated by a linear approximation of Fick's law by applying the following equation:

$$\frac{dq_t}{dt} = Dif(q_{iso} - q_t) \quad (6)$$

where Dif (h^{-1}) is the coefficient of volumetric TC diffusivity in the carbon micropores and q_{iso} (mg g^{-1}) is the equilibrium uptake predicted by the isotherm.

To take into account the existence of a hierarchical porosity, we proposed to evaluate the contribution of the mass transfer for each class of porosity. Therefore, a mathematical expression for the combined intraparticle diffusion, in which the PSD is taken in account, was proposed as follows:

$$\frac{dq_t}{dt} = \sum_{i=1}^{N} Dif_i \left(\frac{S_i}{S_T} q_{iso} - q_i\right) \quad (7)$$

where N is the number of peaks found in the PSD, Dif_i (h^{-1}) is the average diffusivity of the pores at the peak i, S_i and S_T ($m^2\ g^{-1}$) are respectively the area corresponding to the porosity of each peak i and the total surface area accessible to the TC molecules.

Since the models have different numbers of adjustable parameters, the adjusted coefficient of determination was applied to evaluate the performance of each kinetic model. The adjusted coefficient of determination is mathematical related to the traditional R^2 by the following equation [88]:

$$R^2_{Adj} = \frac{(1-R^2)(n_{dat}-1)}{n_{dat}-n_p-1} \quad (8)$$

where R^2 is the traditional coefficient of determination, and n_{dat} and n_p are respectively the numbers of experimental points and adjustable parameters.

2.3.2. Adsorption isotherms

Herein, we applied three isotherm adsorption models: Langmuir, Freundlich and Temkin. Langmuir's model [89] is mathematically represented by:

$$q_{eq} = \frac{q_m \cdot b_L \cdot C_{eq}}{1+b_L \cdot C_{eq}} \quad (9)$$

where C_{eq} (mg L^{-1}) is the liquid phase concentration at equilibrium, q_m (mg g^{-1}) is the maximum monolayer adsorption capacity and b_L (L mg^{-1}) is the Langmuir parameter, related to the free energy of adsorption.

The Freundlich model is mathematically represented by:

$$q_{eq} = K_F C_{eq}^{\frac{1}{n_F}} \quad (10)$$

where K_F ($mg^{1-1/n}\ L^{1/n}\ g^{-1}$) and n_F (dimensionless) are the parameters of the Freundlich model related to the adsorption capacity and adsorption intensity, respectively. In addition, the parameter $1/n_F$ defines if the isotherm is favourable and reversible (values between 0.1 and 1), unfavourable (values above 1.0) or irreversible (values below 0.1) [90,91].

The Temkin model considers that the heat of adsorption decreases when the coverage fraction increases, due to the adsorbate–adsorbent interaction [92]. The Temkin [93] models is represented by:

$$q_{eq} = B \cdot ln\left(K_T \cdot C_{eq}\right) \quad (11)$$

where K_T ($L\ mg^{-1}$) is the Temkin isotherm constant and B ($mg\ g^{-1}$) is the constant related to the heat of adsorption. Usually, B has a positive value, which is indicative of the endothermic character of adsorption in the liquid phase.

The fits of the models to the experimental data were carried out employing as an objective function the sum of the squared errors, Eq. (12), and applying the Nelder-Mead [94] method available in the Maple® software.

$$F_{OBJ} = \sum_{i=1}^{n_{dat}} \left(Y_{i,exp} - Y_{i,mod}\right)^2 \quad (12)$$

where F_{OBJ} is the objective function value, n_{dat} is again the number of experimental points and $Y_{i,exp}$ and $Y_{i,mod}$ are the experimental and predicted values for the experimental point i, respectively.

3. RESULTS AND DISCUSSION

3.1 Materials composition, structural and textural properties

Table 1 shows the elemental composition of raw mimosa tannin (MT) and the two carbon materials derived from MT. The C, H, O and N contents of the latter are close to those already reported in previous studies [39,48,73,95]. Moreover, the ultimate analysis of MT is also in good agreement with the elemental composition of the main flavonoid unit contained in mimosa tannin (Fig. 2).

(a) (b)

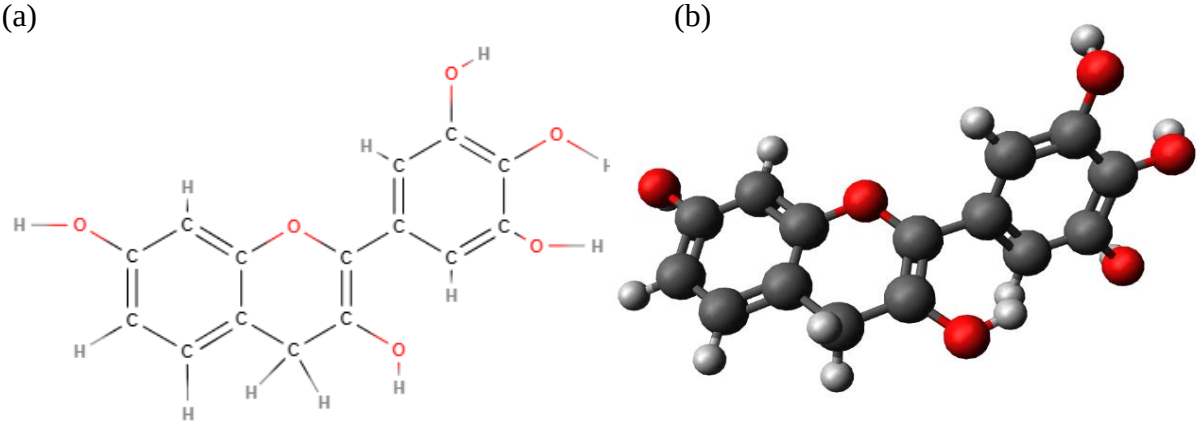

Figure 2. (a) 2D (a) and (b) 3D molecular structure of the main flavonoid unit contained in mimosa tannin[96].

After pyrolysis, there is a carbon enrichment due to heteroatoms evolution by dehydration [97], crosslinking and aromatisation reactions, producing tars and gases [98]. The oxygen content of the carbon produced after hydrothermal treatment (HTC), 11.90 wt.%, is much higher than that of the carbon produced by soft templating (OMC), 3.45 wt.%. This high oxygen content in HTC might lead to a decrease in the TC adsorption capacity [99], since the oxygen content is correlated with the decrease in electron-rich sites in the carbon sheets of the adsorbent, which have high affinity for aromatic compounds [100]. Both carbons show low H, N and S contents, all less than 1.00 wt. %, although HTC has a higher amount of heteroatoms.

Table 1. Elemental analysis of mimosa tannin and derived carbons.

Sample	C (wt. %)	N (wt. %)	H (wt. %)	S (wt. %)	O (wt. %)
Raw mimosa tannin	55.40	0.75	5.00	0.00	38.85
HTC	86.50	0.70	0.90	0.00	11.90
OMC	95.98	0.13	0.44	0.00	3.45

Fig. SI 1 shows the FTIR spectra of HTC and OMC. The peak located around 3400 cm^{-1} is normally related to the presence of hydroxyl groups or to water chemisorbed on the surface, since this wavenumber is attributed to the stretching vibration of O-H group [101,102]. The peaks observed around 1610 and 1010 cm^{-1} are due to the presence of C=C and C–O groups, respectively [102]. The two carbons did not show any of the peaks presents in the FTIR spectrum of their precursor, supporting the low amount of functional groups and hence the poorly developed surface chemistry. This will be supported by the measurements of pH_{PZC}.

The small-angle XRD spectrum of OMC presents one well-resolved band at 2θ = 0.67°, and a shoulder at 2θ = 1.46° (Fig. 3.a). These two values of 2θ correspond to the (100) and (110) reflections, respectively, and this indicates that the carbon has an ordered mesoporous structure belonging to the *P6mm* space group [103,104]. The interplanar spacing, d_{100}, and the unit cell parameter, *a*, calculated for the ordered mesoporous carbon are 13.04 and 15.06 nm, respectively. The scheme given in Fig. 3.a shows the ordered structure of the OMC and its structural parameters d_{100} and *a*. In addition, Fig. 3.b shows the TEM image of the OMC (SI 3 shows that of the HTC), where it is possible to see the hexagonal order of the mesopores. The SEM images of the two carbon materials are shown in Fig. SI 4. Fig. SI 4.a shows the typical microspheres produced when tannin is subjected to hydrothermal treatment [38,39], while the OMC showed a more glassy appearance, with holes and sharp edges, see Fig. SI 4.b.

TC has three acid functional groups [2] (see Fig. 4.a and 4.b) and thus TC exists under different forms of speciation in aqueous solution, depending on the pH, due to protonation-

deprotonation reactions. Fig. 4.d shows the four possible species: H_3TC^+, H_2TC^0, HTC^{-1} and TC^{-2} [105]. Thus, at pH 6, at which the equilibrium and kinetics experiments have been carried out, TC exists mainly in zwitterionic form (i.e., neutral species).

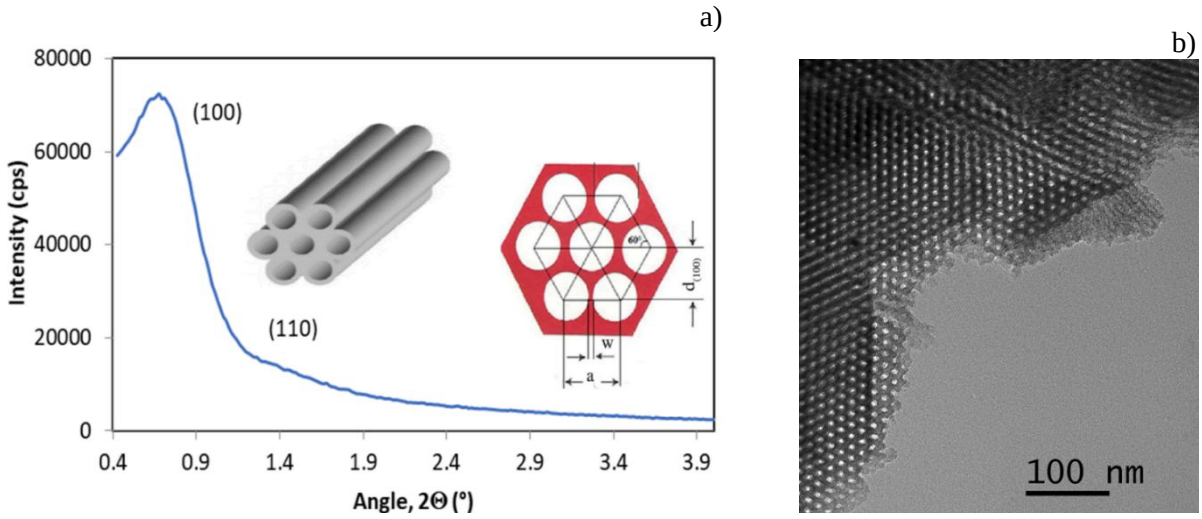

Figure 3. a) Small-angle XRD pattern of the OMC. The insets present a view of the hexagonally ordered mesoporous channels and a cross-section of the structure, showing the structural parameters d_{100} and a. The thickness of the mesopore wall, w, is also shown. b) TEM image of the tannin-based OMC.

The values of pH_{PZC} of HTC and OMC are very similar, 7.0 and 6.6, respectively. At pH below pH_{PZC}, the surface is positively charged due to an excess of H^+ ions, and on the contrary, at pH above pH_{PZC}, the surface of the carbon is negatively charged due to an excess of OH^- ions.

By analysing the results of pH_{PZC} (Fig. 4.c) with the TC speciation diagram (Fig. 4.d), it is possible to identify a narrow region where there are differences in charges between the adsorbate and the adsorbent surface. Due to this, the electrostatic interaction and the hydrogen bonds should not have a significant influence on the adsorption mechanism. Therefore, the π-π electron donor-acceptor interaction between the polarised aromatic rings on the carbon surface and the TC molecule remains the main explanation for the adsorption mechanism [99,106,107].

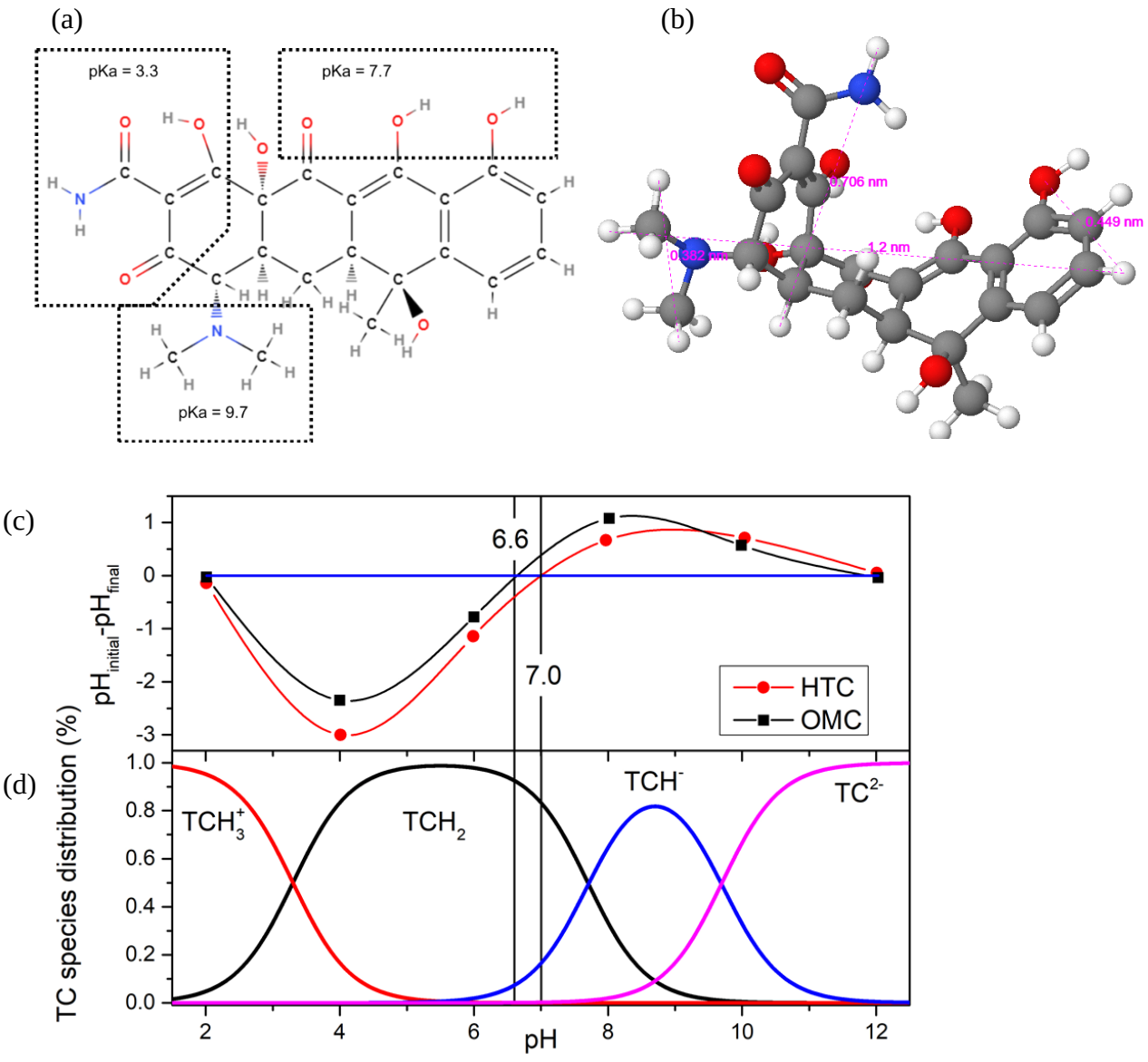

Figure 4. (a) 2D (b) and 3D molecular structure of tetracycline; (c) Determination of the pH_{PZC} of HTC and OMC; and (d) speciation of TC as a function of pH.

Fig. 5.a and 5.b show the N_2 and CO_2 adsorption-desorption isotherms at 77 K and 273 K, respectively, for the two adsorbents. Both N_2 isotherms present a strong increase in the uptake at low pressure, indicating the presence of micropores, characteristic of tannin-derived carbons. The N_2 isotherm of HTC can be classified as type I(a), characteristic of a purely microporous carbon with a very narrow pore size distribution [108]. In contrast, the N_2 isotherm of OMC is a combination of types I (a) and IV(a). Therefore, HTC has only micropores while OMC has micropores and mesopores. This is clearly seen in Fig. 5.c and 5.d, where the PSD per surface area (dS/dw) as well as the cumulated S_{NLDFT} are shown for HTC

and OMC, respectively. In Fig. SI 2, the PSD per volume (dV/dw) and the cumulated volumes are presented, exhibiting the same features as in Fig. 5.c and 5.d. HTC presents a single PSD peak centred at 0.6 nm, more than 99% of the S_{NLDFT} value being due to pores narrower than 1 nm. OMC presents a tri-modal PSD, with contributions to the cumulated S_{NLDFT} of 79, 7 and 13% for pore diameters narrower than 0.9 nm, between 0.9 and 2.4 nm, and wider than 2.4 nm, respectively (see again Fig. 5.d). Similar results have been reported in the literature for other hydrothermal carbons [25,109] and other ordered mesoporous carbons [110–112].

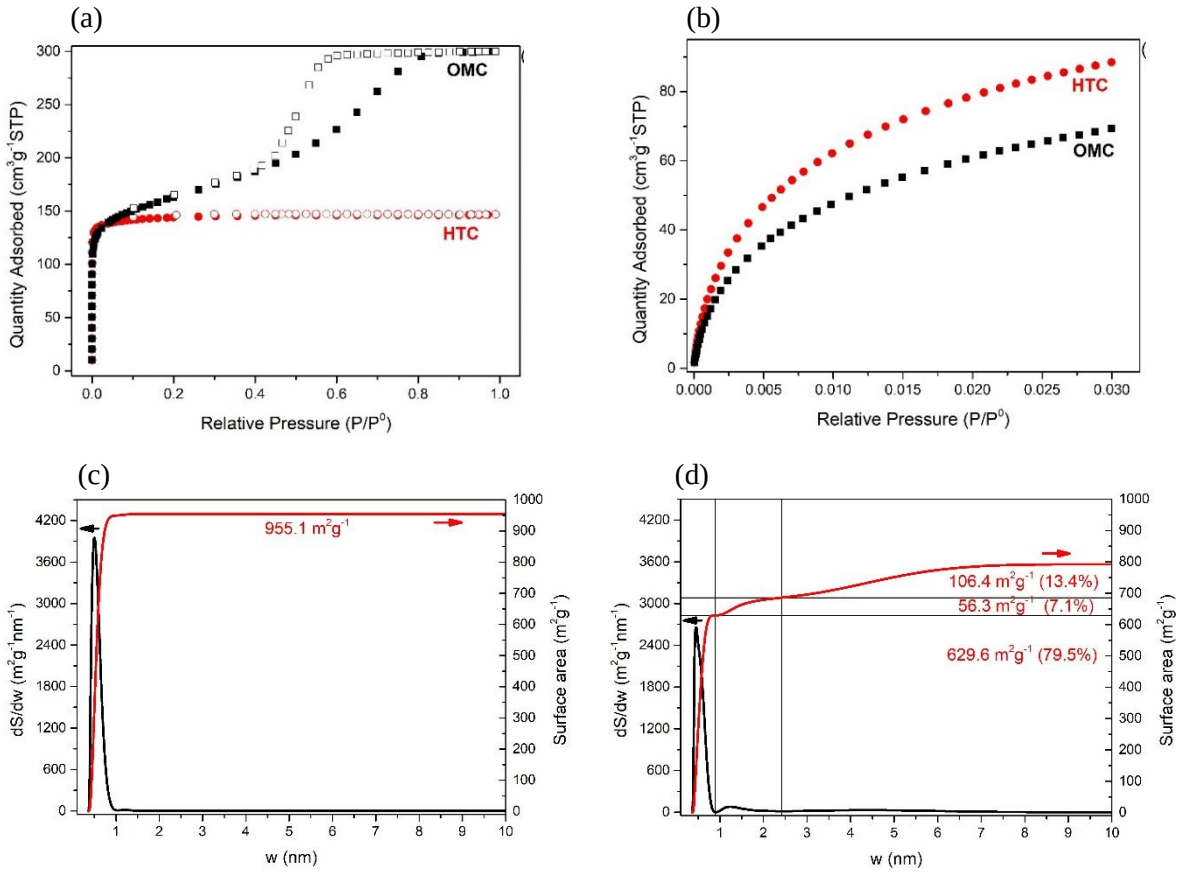

Figure 5. (a) N_2 and (b) CO_2 adsorption/desorption isotherms, where full and empty symbols correspond to adsorption and desorption data, respectively; Pore size distributions and cumulated surface areas S_{NLDFT} of (c) HTC and (d) OMC.

Table 2 shows the textural properties of HTC and OMC. Both carbons have close values of A_{BET}, but HTC has a higher S_{NLDFT}, 955 m^2 g^{-1} compared to 792 m^2 g^{-1} for OMC. This is due to the micropore content of HTC, 0.27 cm^3 g^{-1} (100% of the total pore volume V_T), higher

than that of OMC, 0.20 $cm^3\ g^{-1}$ (44% of V_T), whereas the average micropore size remains the same for both HTC and OMC: 0.6 nm. Nevertheless, OMC presents a pore volume almost twice that of HTC, which is mainly due to mesopores, which represent 56.5% of V_T. The surface area due to mesopores in the OMC is, however, only 113 $m^2\ g^{-1}$.

Table 2. Textural properties of the carbon materials.

Material	A_{BET} ($m^2\ g^{-1}$)	S_{NLDFT} ($m^2\ g^{-1}$)	S_m^* ($m^2\ g^{-1}$)	S_μ^* ($m^2\ g^{-1}$)	$S_{s\mu}^*$ ($m^2\ g^{-1}$)	$S_{u\mu}^*$ ($m^2\ g^{-1}$)	V_T ($cm^3\ g^{-1}$)	V_{meso}^* ($cm^3\ g^{-1}$)	V_μ^* ($cm^3\ g^{-1}$)	$V_{s\mu}^*$ ($cm^3\ g^{-1}$)	$V_{u\mu}^*$ ($cm^3\ g^{-1}$)
HTC	580	955	0.0 (0%)	955 (100%)	92.5 (10%)	862.5 (90%)	0.27	0.0 (0%)	0.27 (100%)	0.04 (15%)	0.23 (85%)
OMC	592	792	113 (14%)	679 (86%)	83.2 (11%)	596.2 (75%)	0.46	0.28 (56%)	0.20 (44%)	0.05 (11%)	0.16 (33%)

* The percentages given in brackets correspond to the contributions of the various pore volumes and surfaces to the total pore volume and surface, respectively $V_{T\ and}$ S_{NLDFT}.

3.2. Tetracycline adsorption

Fig. 6 shows the TC adsorption isotherms at two different temperatures, 288 K and 308 K, together with the fits using Langmuir, Freundlich and Temkin adsorption models.

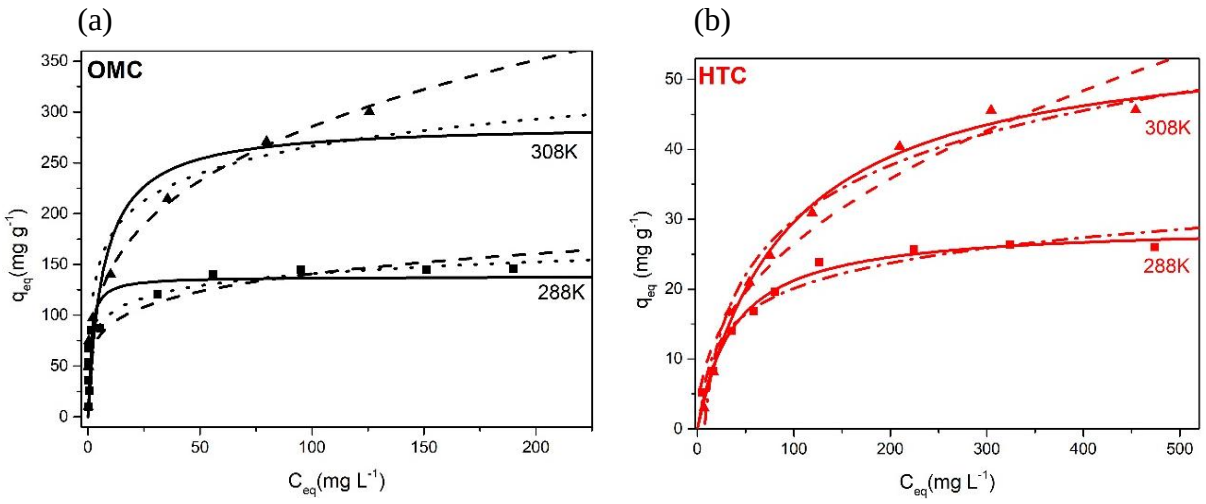

Figure 6. Tetracycline adsorption isotherm on OMC (black) and HTC (red) at 288K (■) and 308K (▲), and their fits by Langmuir (—), Freundlich (--) and Temkin (-·-) models.

The TC adsorption capacity increases with temperature for both carbons. We can also observe that the Freundlich model fits better the TC adsorption isotherms of OMC while the Langmuir model fits better those of HTC. This might be due to the fact that the experimental TC isotherms on HTC and the OMC are type I(a) and mixed types Ia and II, respectively [108].

Table 3 shows the isotherm parameters obtained and the determination coefficients obtained by fitting the models to the experimental data. The TC adsorption capacities of OMC are around 6 times higher than those of HTC. This behaviour cannot be attributed to the surface chemistry, which is quite similar as indicated above, nor to A_{BET} or S_{NLDFT}. The only significant difference between the two carbon materials is their mesopore volume.

Table 3. Estimated parameter values from the fits of the TC isotherms.

T (K)	Langmuir			Freundlich			Temkin		
	q_m (mg g^{-1})	b (L mg^{-1})	R^2	K_F (mg$^{1-1/n}$ L$^{1/n}$ g^{-1})	n	R^2	B (mg g^{-1})	K_T (L mg^{-1})	R^2
OMC									
288	137.9	0.894	0.82	58.4	5.239	0.86	17.0	38.9	0.87
308	288.5	0.146	0.90	72.6	3.363	0.99	38.7	9.8	0.96
HTC									
288	29.2	0.027	0.98	5.04	3.48	0.90	5.26	0.46	0.96
308	56.9	0.011	0.99	3.57	2.30	0.93	11.30	0.14	0.98

As expected for liquid-phase adsorption, the Langmuir monolayer adsorption capacity (q_m) increases with temperature, whereas the adsorption constant (b) decreases. The $1/n$ parameter of the Freundlich model was in all cases in the range corresponding to the favourable and reversible isotherm ($0.1 < 1/n < 1.0$). The parameter B of the Temkim isotherm model increases with the temperature according to the mathematical relationship $B = RT/b_T$[113],

where b_T is a factor related to adsorbent-adsorbate interactions. The Temkim adsorption constant (K_T) follows the same temperature behaviour as that of Langmuir.

Fig. 7 shows the maximum TC adsorption capacities obtained in this study as well as those reported in the literature for other carbons [25,46,48,99,101,105,107,114–119], as a function of either A_{BET} or V_T. The determination coefficient when using A_{BET} is much lower, $R^2 = 0.60$, than that obtained when using V_T, $R^2 = 0.82$. This poor relationship with A_{BET} is because the value of A_{BET} mainly corresponds to the contribution of micropores (pore diameter < 2 nm), which sometimes are not fully accessible to the TC molecules. Moreover, as shown in Fig. 4.b, the size of the TC molecule varies from 0.38 to1.2 nm, depending on its orientation. The better correlation of q_m with V_T could be related to the fact that mesopores and macropores, which are fully accessible to the TC molecule, have a higher impact on the value of V_T. Event like that, the correlation between q_m and V_T is not excellent. A much better correlation should be obtained using the mesopore volumes instead of V_T. Unfortunately, these data are not always available in the open literature.

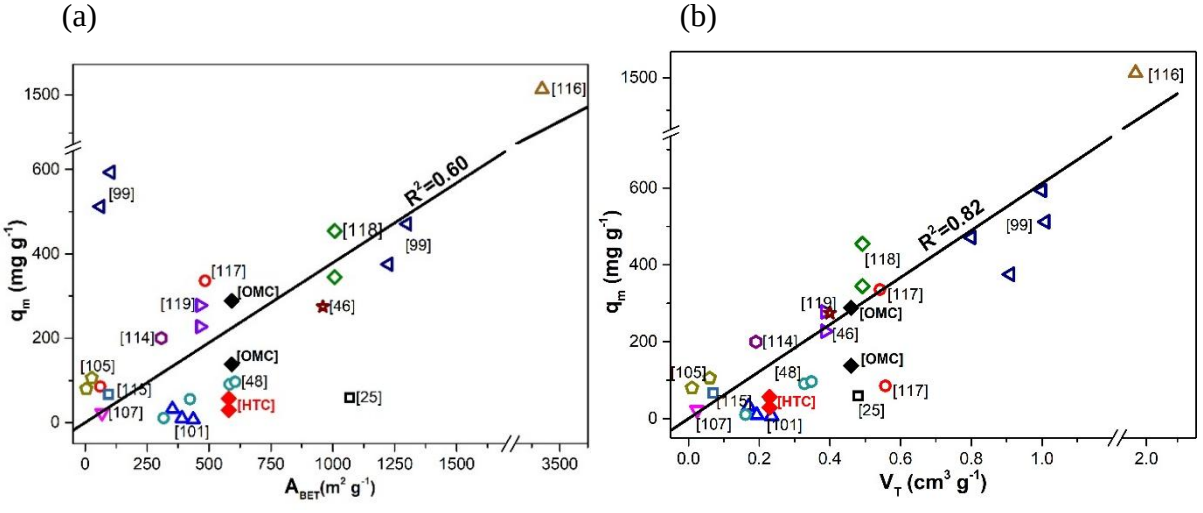

Figure 7. Relationship between the maximum TC adsorption capacity and (a) the BET surface area A_{BET}, or (b) the total pore volume V_T.

Fig. 8 shows the TC uptake at 288 K and 308 K for the two carbon adsorbents as a function of time. The equilibrium was reached after 9 h for both HTC and OMC. The TC adsorption

kinetics on HTC is adequately fitted by the PFO kinetic model. However, the behaviour of TC adsorption kinetics on the OMC is somewhat different but in a good agreement with the results already reported in a previous study [101], where the adsorption of TC on a mesoporous carbon was studied. Taking into account the existence of three different diffusion rates controlling the adsorption kinetics in the OMC, i.e., applying Eq. (7) with N = 3 and assuming that the mass transfer at the mesoporous peak is only governed by external diffusion, the kinetic model proposed takes the form of a Triple Dual Resistance Model (TDRM). This model was able to describe the experimental data with a good accuracy (R^2 > 0.99) for both temperatures, see below.

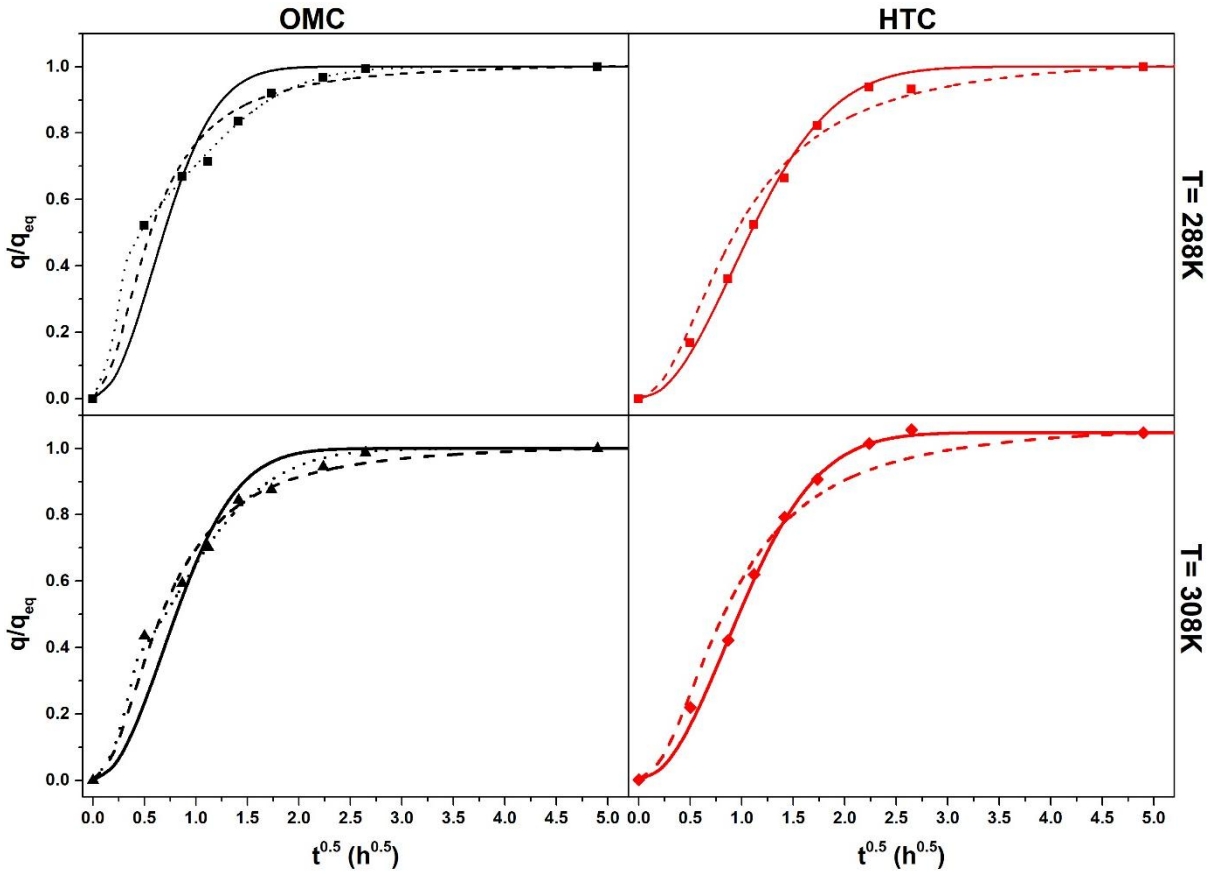

Figure 8. Tetracycline adsorption kinetics on the OMC (black, left) and the HTC (red, right) at 288 K (top) and 308 K (bottom), and the corresponding fits using PFO (—), PSO (--) and TDRM (⋯) models.

Table 4 shows the parameters and determination factors obtained using PFO and PSO kinetic models to fit the experimental data. Although both models are capable of describing the TC adsorption kinetics, PFO model best fits the TC adsorption kinetics on HTC, which may indicate that adsorption is controlled by diffusion into the narrowest pores. PSO best fits the TC adsorption kinetics on OMC, suggesting that external diffusion controls the adsorption rate. Experimental adsorption and modelling results are shown in Fig. 8 (PSO, PFO and TDRM) and Figure SI 5 (other kinetic models).

Table 4. Parameters and determination factors obtained by fitting classical adsorption kinetics models to TC adsorption on HTC and OMC.

	PFO				**PSO**			
	HTC		**OMC**		**HTC**		**OMC**	
T (K)	K_1 (h^{-1})	R^2_{ADj}	K_1 (h^{-1})	R^2_{ADj}	K_2 ($g\,mg^{-1}h^{-1}$)	R^2_{ADj}	K_2 ($g\,mg^{-1}h^{-1}$)	R^2_{ADj}
288	0.59	0.99	1.46	0.89	0.039	0.97	0.023	0.98
308	0.69	1.00	1.07	0.95	0.026	0.97	0.008	0.99

Table 5 shows the parameters obtained by taking into account the contribution of each range of porosity. The traditional dual resistance model (DRM), described by equations (5) and (6), is better adapted to the TC adsorption data on HTC than other conventional models (PFO, PSO) are. However, a triple dual resistance model becomes a better alternative for describing the TC adsorption kinetics on OMC.

Table 5. Parameters and determination factors obtained by fitting dual resistance kinetics models to TC adsorption on HTC and OMC.

	DRM			TDRM				
T (K)	K_f (L g^{-1} h^{-1})	Dif (h^{-1})	R^2_{ADj}	K_f (L g^{-1} h^{-1})	Dif_1 (h^{-1})	Dif_2 (h^{-1})	S (m^2 g^{-1})	R^2_{ADj}
HTC								
288	0.998	0.590	0.99	-	-	-	-	-
308	0.998	0.712	1.00	-	-	-	-	-
OMC								
288	1.16	1.11	0.85	1.35	8.47	0.56	329.9	1.00
308	1.16	1.11	0.94	1.35	15.3	0.67	482.9	1.00

The TDRM allowed us estimating the surface area accessible in the OMC (see Table 5), and the exclusion pore size diameter, i.e., the pore diameter below which the TC molecule cannot access. Such exclusion diameter was calculated from the accessible surface area and the cumulative surface curve shown in Fig. 5.d). The calculation of the latter led to values of 0.54 and 0.59 nm at 308 K and 288 K, respectively. By applying these pore diameters to the PSD of the HTC, it was possible to obtain an estimate of the surface area accessible to TC.

Fig. 9 shows q_m as a function of the theoretical accessible pore volume (APV), obtained from the exclusion pore diameter and the cumulative pore volume shown in Fig. SI 2, and from the total pore volume (V_T) for the two materials of this study and some others from the open literature [25,48,116,117]. There are less points than in Fig. 7 because PSDs were not always available and they are necessary to calculate the APV. q_m follows a linear trend as a function of the V_T (R^2 = 0.65) although the determination factor when representing q_m as a function of APV (R^2 = 0.74) is much better, since the TDRM allows having different APVs at different temperatures for the same adsorbent and discard the pore volume fraction that is not accessible to TC. Therefore, we showed that TDRM provides a tool for understanding how temperature, through changes in the properties of diffusion and fluid dynamics, affect the

maximum amount adsorbed. Moreover, we demonstrated that A_{BET}, although it is easy to calculate and reported by everyone, is not the best tool to evaluate the potential suitability of an adsorbent to remove pollutants in water phase. In this study, we showed, step by step, that V_T is better than A_{BET} and APV still better that V_T.

(a) (b)

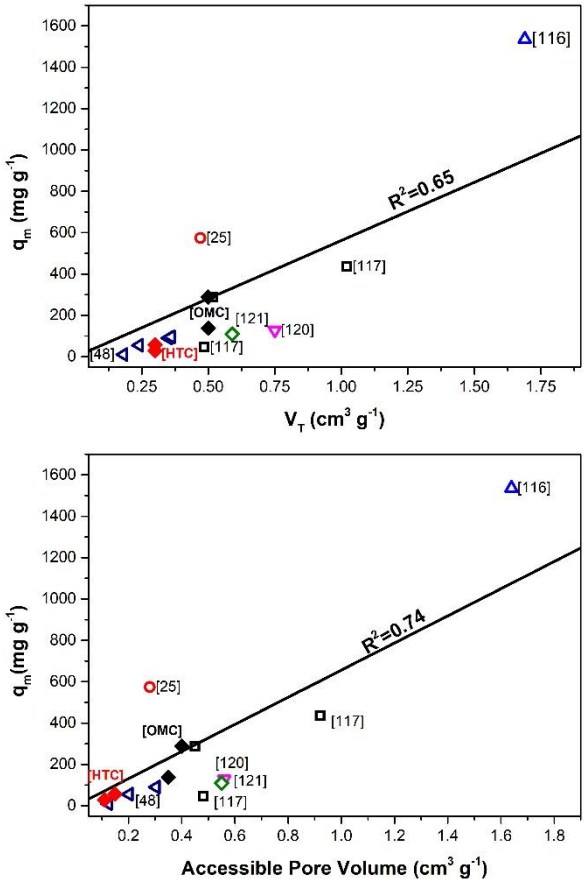

Figure 9. Correlation between the maximum tetracycline adsorption capacity and (a) total and (b) accessible pore volumes.

4. CONCLUSION

Two different carbons were produced by a first step of either hydrothermal treatment or soft templating, to obtain purely microporous (HTC) or micro-mesoporous (OMC) carbon materials, respectively, after pyrolysis at 1173 K. The BET area (A_{BET}) was very similar for

464 the two carbons, but the latter had distinct pore size distribution and total pore volume (V_T).
465 The OMC indeed had an almost two times higher V_T, of which 56.5% were mesopores.

466 Tetracycline (TC) adsorption increased with temperature and the OMC had an adsorption
467 capacity three times higher than the HTC. This difference was attributed to the accessible
468 surface and not to the A_{BET} or the surface chemistry, which are very similar.

469 The kinetics of TC adsorption on OMC was controlled by a combined diffusion in two
470 ranges of micropores and in mesopores, while on HTC it was adequately fitted by a model
471 taking into account the diffusional resistance in the micropores. Moreover, these models
472 allowed estimating the pore size accessible to the TC molecules, and calculate the accessible
473 surface areas and pore volumes (APV). The applied kinetic approach gave an explanation
474 about the better TC adsorption performance of the OMC compared to HTC.

475 We have undoubtedly shown that A_{BET}, while easy to calculate and reported by everyone,
476 is not the best tool to assess the potential suitability of an adsorbent to the removal of TC on
477 carbon materials (e.g. OMC and HTC). V_T is better than A_{BET} and, APV even better than V_T
478 because APV is the accessible pore volume of adsorbent to a given pollutant.

479

480 **Acknowledgements**

481 We gratefully acknowledge the financial support of TALiSMAN project, funded by
482 FEDER (2019-000214). M. Josselin Maurice is thanked for having provided experimental
483 adsorption data obtained during his internship in our lab.

484

485

References

[1] T. Han, Y. Liang, Z. Wu, L. Zhang, Z. Liu, Q. Li, X. Chen, W. Guo, L. Jiang, F. Pan, S. Ge, Z. Mi, Z. Liu, H. Huang, X. Li, J. Zhou, Y. Li, J. Wang, Z. Zhang, Y. Tang, L. Yang, M. Wu, Effects of tetracycline on growth, oxidative stress response, and metabolite pattern of ryegrass, J. Hazard. Mater. 380 (2019) 120885. https://doi.org/10.1016/j.jhazmat.2019.120885.

[2] R. Daghrir, P. Drogui, Tetracycline antibiotics in the environment: A review, Environ. Chem. Lett. 11 (2013) 209–227. https://doi.org/10.1007/s10311-013-0404-8.

[3] H. Xia, J. Chen, X. Chen, K. Huang, Y. Wu, Effects of tetracycline residuals on humification, microbial profile and antibiotic resistance genes during vermicomposting of dewatered sludge, Environ. Pollut. 252 (2019) 1068–1077. https://doi.org/10.1016/j.envpol.2019.06.048.

[4] P. Kay, P.A. Blackwell, A.B.A. Boxall, Transport of veterinary antibiotics in overland flow following the application of slurry to arable land, Chemosphere. 59 (2005) 951–959. https://doi.org/10.1016/j.chemosphere.2004.11.055.

[5] Q. Wang, X. Li, Q. Yang, Y. Chen, B. Du, Evolution of microbial community and drug resistance during enrichment of tetracycline-degrading bacteria, Ecotoxicol. Environ. Saf. 171 (2019) 746–752. https://doi.org/10.1016/j.ecoenv.2019.01.047.

[6] F. Baquero, J.L. Martínez, R. Cantón, Antibiotics and antibiotic resistance in water environments, Curr. Opin. Biotechnol. 19 (2008) 260–265. https://doi.org/10.1016/j.copbio.2008.05.006.

[7] J.A. Atoyan, E.L. Patenaude, D.A. Potts, J.A. Amador, Effects of tetracycline on antibiotic resistance and removal of fecal indicator bacteria in aerated and unaerated leachfield mesocosms, J. Environ. Sci. Heal. - Part A Toxic/Hazardous Subst. Environ. Eng. 42 (2007) 1571–1578. https://doi.org/10.1080/10934520701513498.

[8] L. Wang, Y. Li, W. Ben, J. Hu, Z. Cui, K. Qu, Z. Qiang, In-situ sludge ozone-reduction process for effective removal of fluoroquinolone antibiotics in wastewater treatment plants, Sep. Purif. Technol. 213 (2019) 419–425. https://doi.org/10.1016/j.seppur.2018.12.062.

[9] I.C. Iakovides, I. Michael-Kordatou, N.F.F. Moreira, A.R. Ribeiro, T. Fernandes, M.F.R. Pereira, O.C. Nunes, C.M. Manaia, A.M.T. Silva, D. Fatta-Kassinos,

Continuous ozonation of urban wastewater: Removal of antibiotics, antibiotic-resistant Escherichia coli and antibiotic resistance genes and phytotoxicity, Water Res. 159 (2019) 333–347. https://doi.org/10.1016/j.watres.2019.05.025.

[10] W. Baran, E. Adamek, M. Jajko, A. Sobczak, Removal of veterinary antibiotics from wastewater by electrocoagulation, Chemosphere. 194 (2018) 381–389. https://doi.org/10.1016/j.chemosphere.2017.11.165.

[11] S. Ahmadzadeh, A. Asadipour, M. Pournamdari, B. Behnam, H.R. Rahimi, M. Dolatabadi, Removal of ciprofloxacin from hospital wastewater using electrocoagulation technique by aluminum electrode: Optimization and modelling through response surface methodology, Process Saf. Environ. Prot. 109 (2017) 538–547. https://doi.org/10.1016/j.psep.2017.04.026.

[12] L. Leng, L. Wei, Q. Xiong, S. Xu, W. Li, S. Lv, Q. Lu, L. Wan, Z. Wen, W. Zhou, Use of microalgae based technology for the removal of antibiotics from wastewater: A review, Chemosphere. 238 (2020) 124680. https://doi.org/10.1016/j.chemosphere.2019.124680.

[13] J. Cha, K.H. Carlson, Biodegradation of veterinary antibiotics in lagoon waters, Process Saf. Environ. Prot. 127 (2019) 306–313. https://doi.org/10.1016/j.psep.2019.04.009.

[14] S.F. Pan, M.P. Zhu, J.P. Chen, Z.H. Yuan, L. Bin Zhong, Y.M. Zheng, Separation of tetracycline from wastewater using forward osmosis process with thin film composite membrane - Implications for antibiotics recovery, Sep. Purif. Technol. 153 (2015) 76–83. https://doi.org/10.1016/j.seppur.2015.08.034.

[15] L. Lan, X. Kong, H. Sun, C. Li, D. Liu, High removal efficiency of antibiotic resistance genes in swine wastewater via nanofiltration and reverse osmosis processes, J. Environ. Manage. 231 (2019) 439–445. https://doi.org/10.1016/j.jenvman.2018.10.073.

[16] L. Rizzo, T. Agovino, S. Nahim-Granados, M. Castro-Alférez, P. Fernández-Ibáñez, M.I. Polo-López, Tertiary treatment of urban wastewater by solar and UV-C driven advanced oxidation with peracetic acid: Effect on contaminants of emerging concern and antibiotic resistance, Water Res. 149 (2019) 272–281. https://doi.org/10.1016/j.watres.2018.11.031.

548 [17] S.G. Michael, I. Michael-Kordatou, V.G. Beretsou, T. Jäger, C. Michael, T. Schwartz,
549 D. Fatta-Kassinos, Solar photo-Fenton oxidation followed by adsorption on activated
550 carbon for the minimisation of antibiotic resistance determinants and toxicity present in
551 urban wastewater, Appl. Catal. B Environ. 244 (2019) 871–880.
552 https://doi.org/10.1016/j.apcatb.2018.12.030.

553 [18] X. Peng, F. Hu, T. Zhang, F. Qiu, H. Dai, Amine-functionalized magnetic bamboo-
554 based activated carbon adsorptive removal of ciprofloxacin and norfloxacin: A batch
555 and fixed-bed column study, Bioresour. Technol. 249 (2018) 924–934.
556 https://doi.org/10.1016/j.biortech.2017.10.095.

557 [19] J. Staudt, F.B. Scheufele, C. Ribeiro, T.Y. Sato, R. Canevesi, C.E. Borba,
558 Ciprofloxacin desorption from gel type ion exchange resin: Desorption modeling in
559 batch system and fixed bed column, Sep. Purif. Technol. 230 (2020) 115857.
560 https://doi.org/10.1016/j.seppur.2019.115857.

561 [20] Z. Wang, H. Tang, W. Li, J. Li, R. Xu, K. Zhang, G. He, P.R. Shearing, D.J.L. Brett,
562 Core-shell TiO2@C ultralong nanotubes with enhanced adsorption of antibiotics, J.
563 Mater. Chem. A. 7 (2019) 19081–19086. https://doi.org/10.1039/c9ta06735c.

564 [21] W. Xiong, G. Zeng, Z. Yang, Y. Zhou, C. Zhang, M. Cheng, Y. Liu, L. Hu, J. Wan, C.
565 Zhou, R. Xu, X. Li, Adsorption of tetracycline antibiotics from aqueous solutions on
566 nanocomposite multi-walled carbon nanotube functionalized MIL-53(Fe) as new
567 adsorbent, Sci. Total Environ. 627 (2018) 235–244.
568 https://doi.org/10.1016/j.scitotenv.2018.01.249.

569 [22] G.Z. Kyzas, J. Fu, N.K. Lazaridis, D.N. Bikiaris, K.A. Matis, New approaches on the
570 removal of pharmaceuticals from wastewaters with adsorbent materials, J. Mol. Liq.
571 209 (2015) 87–93. https://doi.org/10.1016/j.molliq.2015.05.025.

572 [23] D.N.R. de Sousa, S. Insa, A.A. Mozeto, M. Petrovic, T.F. Chaves, P.S. Fadini,
573 Equilibrium and kinetic studies of the adsorption of antibiotics from aqueous solutions
574 onto powdered zeolites, Chemosphere. 205 (2018) 137–146.
575 https://doi.org/10.1016/j.chemosphere.2018.04.085.

576 [24] N. Li, L. Zhou, X. Jin, G. Owens, Z. Chen, Simultaneous removal of tetracycline and
577 oxytetracycline antibiotics from wastewater using a ZIF-8 metal organic-framework, J.
578 Hazard. Mater. 366 (2019) 563–572. https://doi.org/10.1016/j.jhazmat.2018.12.047.

579 [25] T. Selmi, A. Sanchez-Sanchez, P. Gadonneix, J. Jagiello, M. Seffen, H. Sammouda, A.
580 Celzard, V. Fierro, Tetracycline removal with activated carbons produced by
581 hydrothermal carbonisation of Agave americana fibres and mimosa tannin, Ind. Crops
582 Prod. 115 (2018) 146–157. https://doi.org/10.1016/j.indcrop.2018.02.005.

583 [26] N. Querejeta, S. García, N. Álvarez-Gutiérrez, F. Rubiera, C. Pevida, Measuring heat
584 capacity of activated carbons for CO2 capture, J. CO2 Util. 33 (2019) 148–156.
585 https://doi.org/10.1016/j.jcou.2019.05.018.

586 [27] F. Yu, Y. Li, S. Han, J. Ma, Adsorptive removal of antibiotics from aqueous solution
587 using carbon materials, Chemosphere. 153 (2016) 365–385.
588 https://doi.org/10.1016/j.chemosphere.2016.03.083.

589 [28] S. Afshin, S.A. Mokhtari, M. Vosoughi, H. Sadeghi, Y. Rashtbari, Data of adsorption
590 of Basic Blue 41 dye from aqueous solutions by activated carbon prepared from
591 filamentous algae, Data Br. 21 (2018) 1008–1013.
592 https://doi.org/10.1016/j.dib.2018.10.023.

593 [29] S. Schaefer, G. Muñiz, M.T. Izquierdo, S. Mathieu, M.L. Ballinas-Casarrubias, G.
594 González-Sánchez, A. Celzard, V. Fierro, Rice straw-based activated carbons doped
595 with SiC for enhanced hydrogen adsorption, Int. J. Hydrogen Energy. 42 (2017)
596 11534–11540. https://doi.org/10.1016/j.ijhydene.2017.02.043.

597 [30] A.H. Basta, V. Fierro, H. El-Saied, A. Celzard, 2-Steps KOH activation of rice straw:
598 An efficient method for preparing high-performance activated carbons, Bioresour.
599 Technol. 100 (2009) 3941–3947. https://doi.org/10.1016/j.biortech.2009.02.028.

600 [31] V. Fierro, G. Muñiz, A.H. Basta, H. El-Saied, A. Celzard, Rice straw as precursor of
601 activated carbons: Activation with ortho-phosphoric acid, J. Hazard. Mater. 181 (2010)
602 27–34. https://doi.org/10.1016/j.jhazmat.2010.04.062.

603 [32] A.H. Basta, V. Fierro, H. Saied, A. Celzard, Effect of deashing rice straws on their
604 derived activated carbons produced by phosphoric acid activation, Biomass and
605 Bioenergy. 35 (2011) 1954–1959. https://doi.org/10.1016/j.biombioe.2011.01.043.

606 [33] Y. Xiang, Z. Xu, Y. Wei, Y. Zhou, X. Yang, Y. Yang, J. Yang, J. Zhang, L. Luo, Z.
607 Zhou, Carbon-based materials as adsorbent for antibiotics removal: Mechanisms and
608 influencing factors, J. Environ. Manage. 237 (2019) 128–138.
609 https://doi.org/10.1016/j.jenvman.2019.02.068.

[34] D.N.K.P. Negara, T.G.T. Nindhia, I.W. Surata, F. Hidajat, M. Sucipta, Nanopore structures, surface morphology, and adsorption capacity of tabah bamboo-activated carbons, Surfaces and Interfaces. 16 (2019) 22–28. https://doi.org/10.1016/j.surfin.2019.04.002.

[35] T.S. Pessôa, L.E. de Lima Ferreira, M.P. da Silva, L.M. Pereira Neto, B.F. do Nascimento, T.J.M. Fraga, E.F. Jaguaribe, J.V. Cavalcanti, M.A. da Motta Sobrinho, Açaí waste beneficing by gasification process and its employment in the treatment of synthetic and raw textile wastewater, J. Clean. Prod. 240 (2019) 118047. https://doi.org/10.1016/j.jclepro.2019.118047.

[36] X. Zhou, Z. Zeng, G. Zeng, C. Lai, R. Xiao, S. Liu, D. Huang, L. Qin, X. Liu, B. Li, H. Yi, Y. Fu, L. Li, Z. Wang, Persulfate activation by swine bone char-derived hierarchical porous carbon: Multiple mechanism system for organic pollutant degradation in aqueous media, Chem. Eng. J. (2019) 123091. https://doi.org/10.1016/j.cej.2019.123091.

[37] A. Jeder, A. Sanchez-Sanchez, P. Gadonneix, E. Masson, A. Ouederni, A. Celzard, V. Fierro, The severity factor as a useful tool for producing hydrochars and derived carbon materials, Environ. Sci. Pollut. Res. 25 (2018) 1497–1507. https://doi.org/10.1007/s11356-017-0366-7.

[38] F.L. Braghiroli, V. Fierro, M.T. Izquierdo, J. Parmentier, A. Pizzi, A. Celzard, Kinetics of the hydrothermal treatment of tannin for producing carbonaceous microspheres, Bioresour. Technol. 151 (2014) 271–277. https://doi.org/10.1016/j.biortech.2013.10.045.

[39] F.L. Braghiroli, V. Fierro, J. Parmentier, L. Vidal, P. Gadonneix, A. Celzard, Hydrothermal carbons produced from tannin by modification of the reaction medium: Addition of H + and Ag +, Ind. Crops Prod. 77 (2015) 364–374. https://doi.org/10.1016/j.indcrop.2015.09.010.

[40] I.A. Khan, A. Badshah, I. Khan, D. Zhao, M.A. Nadeem, Soft-template carbonization approach of MOF-5 to mesoporous carbon nanospheres as excellent electrode materials for supercapacitor, Microporous Mesoporous Mater. 253 (2017) 169–176. https://doi.org/10.1016/j.micromeso.2017.06.049.

[41] X.Y. Chen, L. Zhang, L.X. Cheng, Y.Y. He, Z.J. Zhang, Structure and electrochemical performance of nitrogen-containing nanoporous carbon from diphenylcarbazide via a

template carbonization route, Electrochim. Acta. 142 (2014) 84–91. https://doi.org/10.1016/j.electacta.2014.07.098.

[42] H. Tang, W. Li, H. Jiang, R. Lin, Z. Wang, J. Wu, G. He, P.R. Shearing, D.J.L. Brett, ZIF-8-derived hollow carbon for efficient adsorption of antibiotics, Nanomaterials. 9 (2019). https://doi.org/10.3390/nano9010117.

[43] X. Hu, L. Jia, J. Cheng, Z. Sun, Magnetic ordered mesoporous carbon materials for adsorption of minocycline from aqueous solution: Preparation, characterization and adsorption mechanism, J. Hazard. Mater. 362 (2019) 1–8. https://doi.org/10.1016/j.jhazmat.2018.09.003.

[44] M.R. Benzigar, S.N. Talapaneni, S. Joseph, K. Ramadass, G. Singh, J. Scaranto, U. Ravon, K. Al-Bahily, A. Vinu, Recent advances in functionalized micro and mesoporous carbon materials: Synthesis and applications, Chem. Soc. Rev. 47 (2018) 2680–2721. https://doi.org/10.1039/c7cs00787f.

[45] V.T. Nguyen, T.B. Nguyen, C.W. Chen, C.M. Hung, T.D.H. Vo, J.H. Chang, C. Di Dong, Influence of pyrolysis temperature on polycyclic aromatic hydrocarbons production and tetracycline adsorption behavior of biochar derived from spent coffee ground, Bioresour. Technol. 284 (2019) 197–203. https://doi.org/10.1016/j.biortech.2019.03.096.

[46] H.M. Jang, S. Yoo, Y.K. Choi, S. Park, E. Kan, Adsorption isotherm, kinetic modeling and mechanism of tetracycline on Pinus taeda-derived activated biochar, Bioresour. Technol. 259 (2018) 24–31. https://doi.org/10.1016/j.biortech.2018.03.013.

[47] X. Wei, R. Zhang, W. Zhang, Y. Yuan, B. Lai, High-efficiency adsorption of tetracycline by the prepared waste collagen fiber-derived porous biochar, RSC Adv. 9 (2019) 39355–39366. https://doi.org/10.1039/c9ra07289f.

[48] X. Zhu, C. Li, J. Li, B. Xie, J. Lü, Y. Li, Thermal treatment of biochar in the air/nitrogen atmosphere for developed mesoporosity and enhanced adsorption to tetracycline, Bioresour. Technol. 263 (2018) 475–482. https://doi.org/10.1016/j.biortech.2018.05.041.

[49] M.E. Fernandez, B. Ledesma, S. Román, P.R. Bonelli, A.L. Cukierman, Development and characterization of activated hydrochars from orange peels as potential adsorbents for emerging organic contaminants, Bioresour. Technol. 183 (2015) 221–228.

https://doi.org/10.1016/j.biortech.2015.02.035.

[50] X. Zhu, Y. Liu, C. Zhou, G. Luo, S. Zhang, J. Chen, A novel porous carbon derived from hydrothermal carbon for efficient adsorption of tetracycline, Carbon N. Y. 77 (2014) 627–636. https://doi.org/10.1016/j.carbon.2014.05.067.

[51] R.V.P. Antero, A.C.F. Alves, P. de T. Ferreira Sales, S.B. de Oliveira, S.A. Ojala, S.S. Brum, A new approach to obtain mesoporous-activated carbon via hydrothermal carbonization of Brazilian Cerrado biomass combined with physical activation for bisphenol-A removal, Chem. Eng. Commun. 206 (2019) 1509–1525. https://doi.org/10.1080/00986445.2019.1601625.

[52] L. Ji, F. Liu, Z. Xu, S. Zheng, D. Zhu, Adsorption of pharmaceutical antibiotics on template-synthesized ordered micro- and mesoporous carbons, Environ. Sci. Technol. 44 (2010) 3116–3122. https://doi.org/10.1021/es903716s.

[53] Q. Sui, J. Huang, Y. Liu, X. Chang, G. Ji, S. Deng, T. Xie, G. Yu, Rapid removal of bisphenol A on highly ordered mesoporous carbon, J. Environ. Sci. 23 (2011) 177–182. https://doi.org/10.1016/S1001-0742(10)60391-9.

[54] K.M. González-Ramos, B. Fernández-Reyes, F.R. Román, A.J. Hernández-Maldonado, A hierarchical porous carbon - Mn+[FAU] (Mn+ = Ni2+ or Cu2+) adsorbent: Synthesis, characterization and adsorption of salicylic acid from water, Microporous Mesoporous Mater. 200 (2014) 225–234. https://doi.org/10.1016/j.micromeso.2014.08.055.

[55] B.N. Bhadra, I. Ahmed, S. Kim, S.H. Jhung, Adsorptive removal of ibuprofen and diclofenac from water using metal-organic framework-derived porous carbon, Chem. Eng. J. 314 (2017) 50–58. https://doi.org/10.1016/j.cej.2016.12.127.

[56] K.J. Sreeram, T. Ramasami, Sustaining tanning process through conservation, recovery and better utilization of chromium, Resour. Conserv. Recycl. 38 (2003) 185–212. https://doi.org/10.1016/S0921-3449(02)00151-9.

[57] The Use of Plant Antimicrobial Compounds for Food Preservation, (2015). https://www.hindawi.com/journals/bmri/2015/246264/ (accessed April 16, 2020).

[58] T. Rescigno, M.F. Tecce, A. Capasso, Protective and Restorative Effects of Nutrients and Phytochemicals, Open Biochem. J. 12 (2018) 46–64. https://doi.org/10.2174/1874091x01812010046.

[59] B. Yang, P. Liu, Composition and biological activities of hydrolyzable tannins of fruits of phyllanthus emblica, J. Agric. Food Chem. 62 (2014) 529–541. https://doi.org/10.1021/jf404703k.

[60] T.T. Vu, H. Kim, V.K. Tran, H.D. Vu, T.X. Hoang, J.W. Han, Y.H. Choi, K.S. Jang, G.J. Choi, J.-C. Kim, Antibacterial activity of tannins isolated from Sapium baccatum extract and use for control of tomato bacterial wilt, PLoS One. 12 (2017) e0181499. https://doi.org/10.1371/journal.pone.0181499.

[61] J.F. Harbertson, G.P. Parpinello, H. Heymann, M.O. Downey, Impact of exogenous tannin additions on wine chemistry and wine sensory character, Food Chem. 131 (2012) 999–1008. https://doi.org/10.1016/j.foodchem.2011.09.101.

[62] J. Sánchez-Martín, J. Beltrán-Heredia, C. Solera-Hernández, Surface water and wastewater treatment using a new tannin-based coagulant. Pilot plant trials, J. Environ. Manage. 91 (2010) 2051–2058. https://doi.org/10.1016/j.jenvman.2010.05.013.

[63] K. Li, X. Geng, J. Simonsen, J. Karchesy, Novel wood adhesives from condensed tannins and polyethylenimine, Int. J. Adhes. Adhes. 24 (2004) 327–333. https://doi.org/10.1016/j.ijadhadh.2003.11.004.

[64] A. Pizzl, Condensed tannins for adhesives, Ind. Eng. Chem. Prod. Res. Dev. 21 (1982) 359–369. https://doi.org/10.1021/i300007a005.

[65] V.J. Sealy-Fisher, A. Pizzi, Increased pine tannins extraction and wood adhesives development by phlobaphenes minimization, Holz Als Roh- Und Werkst. 50 (1992) 212–220. https://doi.org/10.1007/BF02663290.

[66] H. Nie, H. Jiang, D. Chong, Q. Wu, C. Xu, H. Zhou, Comparison of water scrubbing and propylene carbonate absorption for biogas upgrading process, Energy and Fuels. 27 (2013) 3239–3245. https://doi.org/10.1021/ef400233w.

[67] Z. Marie, V. Nicolas, A. Celzard, V. Fierro, First approach for modelling the physical foaming of tannin-based thermoset foams, Int. J. Therm. Sci. 149 (2020) 106212. https://doi.org/10.1016/j.ijthermalsci.2019.106212.

[68] Z. Marie, V. Nicolas, A. Celzard, V. Fierro, Experimental investigation of the physical foaming of tannin-based thermoset foams, Ind. Crops Prod. 138 (2019) 111424. https://doi.org/10.1016/j.indcrop.2019.05.073.

[69] G. Tondi, V. Fierro, A. Pizzi, A. Celzard, Tannin-based carbon foams, Carbon N. Y. 47

(2009) 1480–1492. https://doi.org/10.1016/j.carbon.2009.01.041.

[70] G. Amaral-Labat, A. Szczurek, V. Fierro, N. Stein, C. Boulanger, A. Pizzi, A. Celzard, Pore structure and electrochemical performances of tannin-based carbon cryogels, Biomass and Bioenergy. 39 (2012) 274–282. https://doi.org/10.1016/j.biombioe.2012.01.019.

[71] J. Beltrán-Heredia, P. Palo, J. Sánchez-Martín, J.R. Domínguez, T. Gonzáez, Natural adsorbents derived from tannin extracts for pharmaceutical removal in water, Ind. Eng. Chem. Res. 51 (2012) 50–57. https://doi.org/10.1021/ie201017t.

[72] N. Rey-Raap, A. Szczurek, V. Fierro, J.A. Menéndez, A. Arenillas, A. Celzard, Towards a feasible and scalable production of bio-xerogels, J. Colloid Interface Sci. 456 (2015) 138–144. https://doi.org/10.1016/j.jcis.2015.06.024.

[73] F.L. Braghiroli, V. Fierro, M.T. Izquierdo, J. Parmentier, A. Pizzi, A. Celzard, Nitrogen-doped carbon materials produced from hydrothermally treated tannin, Carbon N. Y. 50 (2012) 5411–5420. https://doi.org/10.1016/j.carbon.2012.07.027.

[74] J. Castro-Gutiérrez, N. Díez, M. Sevilla, M.T. Izquierdo, J. Ghanbaja, A. Celzard, V. Fierro, High-Rate Capability of Supercapacitors Based on Tannin-Derived Ordered Mesoporous Carbons, ACS Sustain. Chem. Eng. 7 (2019) 17627–17635. https://doi.org/10.1021/acssuschemeng.9b03407.

[75] F.L. Braghiroli, V. Fierro, M.T. Izquierdo, J. Parmentier, A. Pizzi, L. Delmotte, P. Fioux, A. Celzard, High surface – Highly N-doped carbons from hydrothermally treated tannin, Ind. Crop. Prod. 66 (2015) 282–290. https://doi.org/10.1016/j.indcrop.2014.11.022.

[76] F.L. Braghiroli, V. Fierro, D. Lorraine, P. Seguin, E. Cedex, D. Lorraine, B. Arago, Hydrothermally treated aminated tannin as precursor of N-doped carbon gels for supercapacitors, Carbon N. Y. 90 (2015) 63–74. https://doi.org/10.1016/j.carbon.2015.03.038.

[77] F.L. Braghiroli, V. Fierro, A. Szczurek, N. Stein, J. Parmentier, A. Celzard, Electrochemical performances of hydrothermal tannin-based carbons doped with nitrogen, Ind. Crops Prod. 70 (2015) 332–340. https://doi.org/10.1016/j.indcrop.2015.03.046.

[78] A. Sanchez-Sanchez, M.T. Izquierdo, G. Medjahdi, J. Ghanbaja, A. Celzard, V. Fierro,

Ordered mesoporous carbons obtained by soft-templating of tannin in mild conditions, Microporous Mesoporous Mater. 270 (2018) 127–139. https://doi.org/10.1016/j.micromeso.2018.05.017.

[79] C. Yao, T. Chen, A new simplified method for estimating film mass transfer and surface diffusion coefficients from batch adsorption kinetic data, Chem. Eng. J. 265 (2015) 93–99. https://doi.org/10.1016/j.cej.2014.12.005.

[80] M.G. Sausen, F.B. Scheufele, H.J. Alves, M.G.A. Vieira, M.G.C. da Silva, F.H. Borba, C.E. Borba, Efficiency maximization of fixed-bed adsorption by applying hybrid statistical-phenomenological modeling, Sep. Purif. Technol. 207 (2018) 477–488. https://doi.org/10.1016/j.seppur.2018.07.002.

[81] S. Lagergren, Zur theorie der sogenannten adsorption geloster stoffe, K. Sven. Vetenskapsakad. Handl. 24 (1898) 1–39.

[82] Y.S. Ho, G. McKay, Pseudo-second order model for sorption process, Process Biochem. 34 (1999) 451–465.

[83] P.J.M. Carrott, J.M.V. Nabais, M.M.L. Ribeiro Carrott, J.A. Menéndez, Thermal treatments of activated carbon fibres using a microwave furnace, Microporous Mesoporous Mater. 47 (2001) 243–252. https://doi.org/10.1016/S1387-1811(01)00384-5.

[84] S. Brunauer, P.H. Emmett, E. Teller, Adsorption of Gases in Multimolecular Layers, J. Am. Chem. Soc. 60 (1938) 309–319. https://doi.org/10.1021/ja01269a023.

[85] J. Jagiello, C. Ania, J.B. Parra, C. Cook, Dual gas analysis of microporous carbons using 2D-NLDFT heterogeneous surface model and combined adsorption data of N2 and CO2, Carbon N. Y. 91 (2015) 330–337. https://doi.org/10.1016/j.carbon.2015.05.004.

[86] J. Jagiello, J. Kenvin, A. Celzard, V. Fierro, Enhanced resolution of ultra micropore size determination of biochars and activated carbons by dual gas analysis using N2 and CO2 with 2D-NLDFT adsorption models, Carbon N. Y. 144 (2019) 206–215. https://doi.org/10.1016/j.carbon.2018.12.028.

[87] J. Ma, Z. Jiang, J. Cao, F. Yu, Enhanced adsorption for the removal of antibiotics by carbon nanotubes/graphene oxide/sodium alginate triple-network nanocomposite hydrogels in aqueous solutions, Chemosphere. 242 (2020) 125188.

https://doi.org/10.1016/j.chemosphere.2019.125188.

[88] J. Miles, R Squared, Adjusted R Squared, Wiley StatsRef Stat. Ref. Online. (2014) 2–4. https://doi.org/10.1002/9781118445112.stat06627.

[89] I. Langmuir, The constitution and fundamental properties of solids and liquids. Part I. Solids, J. Am. Chem. Soc. 38 (1916) 2221–2295. https://doi.org/10.1021/ja02268a002.

[90] Y. Zhou, X. Liu, Y. Xiang, P. Wang, J. Zhang, F. Zhang, J. Wei, L. Luo, M. Lei, L. Tang, Modification of biochar derived from sawdust and its application in removal of tetracycline and copper from aqueous solution: Adsorption mechanism and modelling, Bioresour. Technol. 245 (2017) 266–273. https://doi.org/10.1016/j.biortech.2017.08.178.

[91] R. Saadi, Z. Saadi, R. Fazaeli, N.E. Fard, Monolayer and multilayer adsorption isotherm models for sorption from aqueous media, Korean J. Chem. Eng. 32 (2015) 787–799. https://doi.org/10.1007/s11814-015-0053-7.

[92] N. Ayawei, A.N. Ebelegi, D. Wankasi, Modelling and Interpretation of Adsorption Isotherms, J. Chem. 2017 (2017). https://doi.org/10.1155/2017/3039817.

[93] M. Temkin, V. Pyzhev, Kinetics of Ammonia Synthesis on Promoted Iron, Acta Physicochim. URSS. 12 (1940) 217–222.

[94] J.A. Nelder, R. Mead, A simplex method for function minimization, Comput. J. 7 (1964) 308–313. https://doi.org/10.1093/comjnl/7.4.308.

[95] R.W. Chang, C.J. Lin, S.Y.H. Liou, M.A. Bañares, M.O. Guerrero-Pérez, R.M. Martín Aranda, Enhanced cyclic CO2/N2 separation performance stability on chemically modified N-doped ordered mesoporous carbon, Catal. Today. (2019). https://doi.org/10.1016/j.cattod.2019.08.004.

[96] F. Braghiroli, V. Fierro, A. Pizzi, K. Rode, W. Radke, L. Delmotte, J. Parmentier, A. Celzard, Reaction of condensed tannins with ammonia, Ind. Crops Prod. 44 (2013) 330–335. https://doi.org/10.1016/j.indcrop.2012.11.024.

[97] S. Schaefer, V. Fierro, M.T. Izquierdo, A. Celzard, Assessment of hydrogen storage in activated carbons produced from hydrothermally treated organic materials, Int. J. Hydrogen Energy. 41 (2016) 12146–12156. https://doi.org/10.1016/j.ijhydene.2016.05.086.

827 [98] M.J. Ahmed, Adsorption of quinolone, tetracycline, and penicillin antibiotics from
828 aqueous solution using activated carbons: Review, Environ. Toxicol. Pharmacol. 50
829 (2017) 1–10. https://doi.org/10.1016/j.etap.2017.01.004.

830 [99] J. Rivera-Utrilla, C. V. Gómez-Pacheco, M. Sánchez-Polo, J.J. López-Peñalver, R.
831 Ocampo-Pérez, Tetracycline removal from water by adsorption/bioadsorption on
832 activated carbons and sludge-derived adsorbents, J. Environ. Manage. 131 (2013) 16–
833 24. https://doi.org/10.1016/j.jenvman.2013.09.024.

834 [100] C.A. Leon y Leon, J.M. Solar, V. Calemma, L.R. Radovic, Evidence for the
835 protonation of basal plane sites on carbon, Carbon N. Y. 30 (1992) 797–811.
836 https://doi.org/10.1016/0008-6223(92)90164-R.

837 [101] S. Álvarez-Torrellas, R.S. Ribeiro, H.T. Gomes, G. Ovejero, J. García, Removal of
838 antibiotic compounds by adsorption using glycerol-based carbon materials, Chem. Eng.
839 J. 296 (2016) 277–288. https://doi.org/10.1016/j.cej.2016.03.112.

840 [102] G. Tondi, M. Link, C.W. Oo, A. Petutschnigg, A simple approach to distinguish classic
841 and formaldehyde-free tannin based rigid foams by ATR FT-IR, J. Spectrosc. 2015
842 (2015). https://doi.org/10.1155/2015/902340.

843 [103] S. Jun, Sang Hoon Joo, R. Ryoo, M. Kruk, M. Jaroniec, Z. Liu, T. Ohsuna, O. Terasaki,
844 Synthesis of new, nanoporous carbon with hexagonally ordered mesostructure [5], J.
845 Am. Chem. Soc. 122 (2000) 10712–10713. https://doi.org/10.1021/ja002261e.

846 [104] D. Zhao, J. Feng, Q. Huo, N. Melosh, G.H. Fredrickson, B.F. Chmelka, G.D. Stucky,
847 Triblock Copolymer Syntheses of Mesoporous, Science (80-.). 279 (1998) 548–552.

848 [105] Y. Kong, Y. Zhuang, K. Han, B. Shi, Enhanced tetracycline adsorption using alginate-
849 graphene-ZIF67 aerogel, Colloids Surfaces A Physicochem. Eng. Asp. 588 (2020)
850 124360. https://doi.org/10.1016/j.colsurfa.2019.124360.

851 [106] W. Yang, F. Zheng, Y. Lu, X. Xue, N. Li, Adsorption interaction of tetracyclines with
852 porous synthetic resins, Ind. Eng. Chem. Res. 50 (2011) 13892–13898.
853 https://doi.org/10.1021/ie202166g.

854 [107] P. Liao, Z. Zhan, J. Dai, X. Wu, W. Zhang, K. Wang, S. Yuan, Adsorption of
855 tetracycline and chloramphenicol in aqueous solutions by bamboo charcoal: A batch
856 and fixed-bed column study, Chem. Eng. J. 228 (2013) 496–505.
857 https://doi.org/10.1016/j.cej.2013.04.118.

858 [108] M. Thommes, K. Kaneko, A. V. Neimark, J.P. Olivier, F. Rodriguez-Reinoso, J.
859 Rouquerol, K.S.W. Sing, Physisorption of gases, with special reference to the
860 evaluation of surface area and pore size distribution (IUPAC Technical Report), Pure
861 Appl. Chem. 87 (2015) 1051–1069. https://doi.org/10.1515/pac-2014-1117.

862 [109] Y. Shi, X. Zhang, G. Liu, Activated Carbons Derived from Hydrothermally Carbonized
863 Sucrose: Remarkable Adsorbents for Adsorptive Desulfurization, ACS Sustain. Chem.
864 Eng. 3 (2015) 2237–2246. https://doi.org/10.1021/acssuschemeng.5b00670.

865 [110] D. Wu, Y. Liangs, X. Yang, C. Zou, Z. Li, G. Lv, X. Zeng, R. Fu, Preparation of
866 activated ordered mesoporous carbons with a channel structure, Langmuir. 24 (2008)
867 2967–2969. https://doi.org/10.1021/la703511z.

868 [111] X. Wang, J.S. Lee, Q. Zhu, J. Liu, Y. Wang, S. Dai, Ammonia-treated ordered
869 mesoporous carbons as catalytic materials for oxygen reduction reaction, Chem. Mater.
870 22 (2010) 2178–2180. https://doi.org/10.1021/cm100139d.

871 [112] A. Castro-Muñiz, S. Lorenzo-Fierro, A. Martínez-Alonso, J.M.D. Tascón, V. Fierro, F.
872 Suárez-García, J.I. Paredes, Ordered mesoporous carbons obtained from low-value coal
873 tar products for electrochemical energy storage and water remediation, Fuel Process.
874 Technol. 196 (2019) 106152. https://doi.org/10.1016/j.fuproc.2019.106152.

875 [113] A. Şeker, T. Shahwan, A.E. Eroğlu, S. Yilmaz, Z. Demirel, M.C. Dalay, Equilibrium,
876 thermodynamic and kinetic studies for the biosorption of aqueous lead(II), cadmium(II)
877 and nickel(II) ions on Spirulina platensis, J. Hazard. Mater. 154 (2008) 973–980.
878 https://doi.org/10.1016/j.jhazmat.2007.11.007.

879 [114] M.H. Marzbali, M. Esmaieli, H. Abolghasemi, M.H. Marzbali, Tetracycline adsorption
880 by H3PO4-activated carbon produced from apricot nut shells: A batch study, Process
881 Saf. Environ. Prot. 102 (2016) 700–709. https://doi.org/10.1016/j.psep.2016.05.025.

882 [115] J. Liu, B. Zhou, H. Zhang, J. Ma, B. Mu, W. Zhang, A novel Biochar modified by
883 Chitosan-Fe/S for tetracycline adsorption and studies on site energy distribution,
884 Bioresour. Technol. 294 (2019) 122152.
885 https://doi.org/10.1016/j.biortech.2019.122152.

886 [116] J. Yang, J. Dai, L. Wang, W. Ge, A. Xie, J. He, Y. Yan, Ultrahigh adsorption of
887 tetracycline on willow branche-derived porous carbons with tunable pore structure:
888 Isotherm, kinetics, thermodynamic and new mechanism study, J. Taiwan Inst. Chem.

Eng. 96 (2019) 473–482. https://doi.org/10.1016/j.jtice.2018.12.017.

[117] R. Acosta, V. Fierro, A. Martinez de Yuso, D. Nabarlatz, A. Celzard, Tetracycline adsorption onto activated carbons produced by KOH activation of tyre pyrolysis char, Chemosphere. 149 (2016) 168–176. https://doi.org/10.1016/j.chemosphere.2016.01.093.

[118] L. Huang, C. Shi, B. Zhang, S. Niu, B. Gao, Characterization of Activated Carbon Fiber by Microwave Heating and the Adsorption of Tetracycline Antibiotics, Sep. Sci. Technol. 48 (2013) 1356–1363. https://doi.org/10.1080/01496395.2012.732978.

[119] Q. Yang, P. Wu, J. Liu, S. Rehman, Z. Ahmed, B. Ruan, N. Zhu, Batch interaction of emerging tetracycline contaminant with novel phosphoric acid activated corn straw porous carbon: Adsorption rate and nature of mechanism, Environ. Res. 181 (2020) 108899. https://doi.org/10.1016/j.envres.2019.108899.

[120] M.J. Ahmed, M.A. Islam, M. Asif, B.H. Hameed, Human hair-derived high surface area porous carbon material for the adsorption isotherm and kinetics of tetracycline antibiotics, Bioresour. Technol. 243 (2017) 778–784. https://doi.org/10.1016/j.biortech.2017.06.174.

[121] N. Boudrahem, S. Delpeux-Ouldriane, L. Khenniche, F. Boudrahem, F. Aissani-Benissad, M. Gineys, Single and mixture adsorption of clofibric acid, tetracycline and paracetamol onto Activated carbon developed from cotton cloth residue, Process Saf. Environ. Prot. 111 (2017) 544–559. https://doi.org/10.1016/j.psep.2017.08.025.